PCCP

Accepted Manuscript

This article can be cited before page numbers have been issued, to do this please use: H. Zeng, Y. Gu, G. Teng, Y. Liu, J. Zheng and F. Pan, *Phys. Chem. Chem. Phys.*, 2018, DOI: 10.1039/C8CP01949E.

View Article Online
DOI: 10.1039/C8CP01949E

Journal Name

ARTICLE

Ab Initio Identification of Li-Rich Phase in $LiFePO_4$

Hua Zeng,[a] Yue Gu,[a] Gaofeng Teng,[a] Yimeng Liu,[a] Jiaxin Zheng,*[a] and Feng Pan*[a]

Received 00th January 20xx,
Accepted 00th January 20xx

DOI: 10.1039/x0xx00000x

www.rsc.org/

Recent discovery of anionic redox activity in Li-rich layered compounds opens a new direction for the design of high-capacity cathode materials for lithium-ion batteries. Here using extensive ab initio calculations, the thermodynamic existence of Li-rich phase in $LiFePO_4$ to form $Li_{1+x}Fe_{1-x}PO_4$ with *x* not exceeding 12.5% has been proved. Anionic redox and structural stability during delithiation are further investigated. Interestingly, it is found that $Li_{1+x}Fe_{1-x}PO_4$ cannot be delithiated completely and thus cannot achieve extra capacity by anionic redox activity, because the local oxygen-ion redox will cause the fracture of the rigid framework formed by phosphate tetrahedral polyanion. Although the extra capacity cannot be realized, the excess Li-ions at Fe sites can enhance the Li-ion diffusivity along the adjacent [010] channel, and contribute to the shift from 1D to 2D/3D diffusion. This study provides a fresh perspective on olivine-type $LiFePO_4$, and offers some important clues on designing Li-rich cathode materials with high energy density.

Introduction

With the rapid development of transportation applications, including hybrid electric vehicles, plug-in hybrid electric vehicles (PEVs) and pure electric vehicles (EVs), batteries with high energy density are urgently demanded.[1, 2] Developing anode and cathode materials with high energy density for rechargeable lithium-ion batteries (LIBs) becomes the most important way to meet such requirement.[3] LIB anodes, such as a new graphene allotrope known as graphenylene,[4] heteroatom-doped graphene,[5] and a compound of highly dispersed nano structured carbon nanotubes (CNTs), graphene nanoplatelet (GNPs) flakes and carbon nanofibers (CNFs),[6] have been found to be capable of storing lithium with higher energy density. For LIB cathode materials, traditional cathode materials have relied on cationic redox reactions, and transition metals (TM) have been considered as the sole source of electrochemical activity in an intercalation cathode to provide the charge-compensating electrons after Li-ion extraction.[7-11] As a consequence, the theoretical specific capacity is limited by the number of electrons that the TM ions can exchange per unit mass. Recently, with the discovery of anionic redox activity in Li-rich layered compounds, a new design paradigm for LIB cathodes based on a cumulative cationic and anionic redox activity has attracted increasing interests.[12-14] The anionic redox activity will create extra capacity beyond the theoretical TM redox capacity at a high voltage, thus to extend the design of new high-capacity cathodes. Previous reported anionic redox activities are mainly observed within the Li-excess layered TM oxides, such as layered NMC (Ni–Mn–Co),[15-17] Li_2MnO_3,[18-20] $Li_{1.2}Ni_{0.2}Mn_{0.6}O_2$,[21] $Li_{1.3}Nb_{0.3}Me_{0.4}O_2$ (Me = Fe^{3+}, Mn^{3+} and V^{3+}),[22, 23] $Li_2Ru_{1-y}Sn_yO_3$,[24, 25] Li_4FeSbO_6,[26] Li_8ZrO_6,[27] α-Li_2IrO_3,[28] β-Li_2IrO_3,[29] and Li_3IrO_4.[30]

One critical issue of the practical application for the reported Li-rich layered materials is the capacity fading during electrochemical cycles, due to the irreversible loss of lattice oxygen during the anionic redox process.[31, 32] It will be interesting to know whether there is possibility to form Li-rich phase in polyanionic intercalation TM compounds (e.g., $LiFePO_4$ and Li_2FeSiO_4), as the strong P-O and Si-O covalence can stabilize the lattice oxygen during the anionic redox process. Li-rich solid solution of $Li_{2+2x}Fe_{1-x}SiO_4$ ($0 \le x \le 0.3$) is reported recently,[33] but the presence of additional Li-ions are in interstitial sites, which are different from the Li-rich layered materials with additional Li-ions occupying the TM sites. Moreover, no extra capacity in $Li_{2+2x}Fe_{1-x}SiO_4$ is reported. Actually, Li_2FeSiO_4 itself can be regarded as a kind of materials with anionic redox activity, as during the delithiation of the second Li-ion, oxygen redox happens.[34] In the crystal structure of $LiFePO_4$ (LFP), an important commercialized cathode material for rechargeable LIBs,[35-37] all of the oxygen-ions form strong covalent bonds with phosphorus to form the phosphate tetrahedral polyanion and generate a stable three-dimensional framework.[38] If the Li-rich phase exists, better structural stability compared with the reported Li-rich layered materials would be anticipated when the anionic redox happens, thus leading to stable extra reversible lithium storage capacity beyond the theoretical value of LFP. Though the Li-excess $Li_{1.05}Fe_{0.95}PO_4$ is recently synthesized,[39] they mainly focus on the influence of the excess Li-ions (at Fe sites) on the Li-Fe anti-site defects and don't pay attention to the possibility of anionic redox activity.

In this work, using extensive ab initio calculations, we have proved the thermodynamic existence of $Li_{1+x}Fe_{1-x}PO_4$ ($0 \le x \le 12.5\%$). Interestingly, the extra capacity beyond the theoretical value of LFP cannot be achieved by the Li-rich phase, due to the structural

[a] School of Advanced Materials, Peking University, Shenzhen Graduate School, Shenzhen 518055, People's Republic of China.
*Corresponding Authors: zhengjx@pkusz.edu.cn and panfeng@pkusz.edu.cn

View Article Online
DOI: 10.1039/C8CP01949E

instability when the content of the extracted Li-ions exceeds (1-2*x*). Further analysis reveals that the structural instability can be attributed to that the local oxygen-ion redox will cause the fracture of the rigid framework formed by phosphate tetrahedral polyanion. Nevertheless, the Li-ion diffusivity in $Li_{1+x}Fe_{1-x}PO_4$ can be enhanced by the excess Li-ions at Fe sites, reflected by the reduced energy barrier for the Li-ion diffusion along the adjacent [010] channel and the shift from 1D to 2D/3D diffusion. Our findings provide a fresh perspective on olivine-type $LiFePO_4$, and offer some important clues on designing Li-rich cathode materials with high energy density.

Calculation method

All calculations were performed using the plane-wave projector-augmented wave method, as implemented in the Vienna Ab Initio Simulation Package (VASP). The Perdew−Burke−Ernzerhof (PBE) form of generalized gradient approximation (GGA) was chosen as the exchange-correlation potential.[40] Taking account of the strong on-site Coulomb interaction (U) presented in the localized 3d electrons of Fe, the PBE+U approach was employed with the U value set to 5.3 eV in $Li_{1+x}Fe_{1-x}PO_4$.[41, 42]

Geometry optimizations and total energy calculations were spin-polarized, using a plane-wave cutoff of 520 eV. A ferromagnetic high-spin Fe state was assumed, and the energetic effects of the magnetic ordering were small (< 0.04 eV). All the atomic positions and cell parameters were fully relaxed using a conjugate gradient algorithm, until the force on each atom was smaller than 0.01 eV/Å, and energies were converged to within 10^{-5} eV per atom. A 4×3×4 k-point grid within the Monkhorst−Pack scheme was used to sample the Brillouin zone of the $Li_{1+x}Fe_{1-x}PO_4$ supercell. The supercell containing 1×2×2 unit cells (space group *Pnma*) was used, which corresponded to 112 atoms/cell.

A climbing-image nudged elastic band (cNEB) method was used to calculate the energy barriers for Li-ion diffusion in the bulk $Li_{1+x}Fe_{1-x}PO_4$. The nudged elastic band (NEB) is a method for finding saddle point and minimum energy path between known initial state and final state. This method works by optimizing a number of intermediate images along the path. Each image finds the lowest energy possible while maintaining equal spacing to neighboring images. The cNEB method is a small modification to the NEB method in which the highest energy image is driven up to the saddle point. This image does not feel the spring forces along the band. Instead, the true force at this image along the tangent is inverted. In this way, the image tries to maximize its energy along the band, and minimize in all other directions. When this image converges, it will be at the exact saddle point.[43] Initial state is a configuration with a Li-vacancy at one of octahedral sites and a Li-ion at adjacent octahedral site. Final state is opposite to initial state. Five intermediate states are inserted. All ions were relaxed for calculations of the minimum energy pathways.

The density functional perturbation theory (DFPT) was used for phonon calculations.[44] All the atomic positions were fully relaxed until the force on each atom was smaller than 0.001 eV/Å, and energies were converged to within 10^{-8} eV per atom. Phonopy was used to handle force constants gained by DFPT.

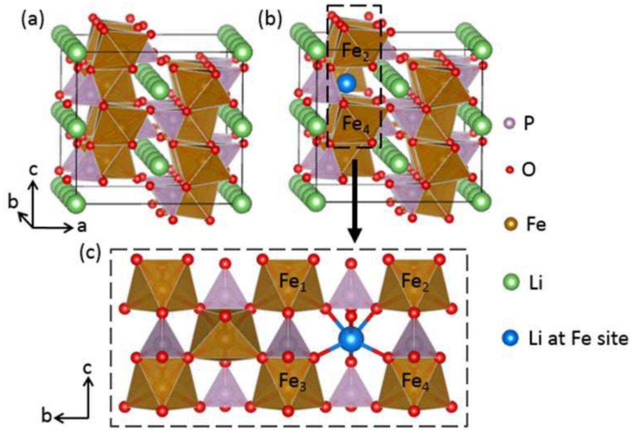

Figure 1. (a) Schematic for the structure of $LiFePO_4$. (b) Schematic for the structure of $Li_{1+x}Fe_{1-x}PO_4$ (*x* = 6.25%). (c) The structure configuration around the excess Li-ion at Fe site in *bc* plane (without considering Li-ions in the [010] channel).

Results and discussion

The existence of Li-Rich phase in $LiFePO_4$.

Figure 1a shows the crystal structure of olivine-type $LiFePO_4$. It was reported to crystallize in the orthorhombic space group *Pnma* with *a* = 10.3377, *b* = 6.0112, and *c* = 4.6950 Å.[45] Correspondingly, for 1×2×2 supercell, *a*, *b*, and *c* should be 10.3377, 12.0224, and 9.390 Å, respectively. As shown in Table 1, the calculated lattice parameters of $LiFePO_4$ are *a* = 10.447, *b* = 12.170 and *c* = 9.507 Å, in satisfactory agreement with the experimental values. We constructed the initial structures of $Li_{1+x}Fe_{1-x}PO_4$ (*x* = 6.25% and 12.5%) by replacing Fe-ions with Li-ions. In $LiFePO_4$, all Fe-ions are coordinated with six oxygen-ions to form the FeO_6 octahedra, which are connected by sharing O corners to form a 2D network in *bc* plane. All Fe sites are equivalent, and thus there is only one doping structure when *x* is 6.25% (Figure 1b). For *x* = 12.5%, there are a lot

Table 1. The variation of lattice parameters, volume and calculated formation energy of $Li_{1+x}Fe_{1-x}PO_4$.

x	*a* [Å]	*b* [Å]	*c* [Å]	α [°]	β [°]	γ [°]	V [Å^3]	ΔH_f [eV/f.u.]
0	10.447	12.170	9.507	90.00	90.00	90.00	1208.77	-12.488
6.25%	10.420	12.146	9.504	90.00	90.11	90.00	1202.81	-12.677
12.5%	10.380	12.128	9.508	90.00	90.13	90.00	1196.98	-12.908
18.75%	10.366	12.083	9.506	90.00	90.30	90.00	1190.71	-13.130

View Article Online
DOI: 10.1039/C8CP01949E

of doping structures. By comparing the total energies of them, we chose the structure with the minimum total energy for the further studies. All structures of $Li_{1+x}Fe_{1-x}PO_4$ (x = 12.5%) are displayed in Figure S1. The structure of $Li_{1+x}Fe_{1-x}PO_4$ (x = 18.75%) is displayed in Figure S2.

Table 1 shows the variation of lattice parameters and volume of $Li_{1+x}Fe_{1-x}PO_4$ after structural optimization. With the increase of x, a and b lattices shrink a little, c keeps nearly invariant, and the volume gets smaller as well. Moreover, the excess Li-ions at Fe sites change the structural symmetry, resulting in a slight structural tilt with the β angle exceeding 90°.

To study the thermodynamic stability of $Li_{1+x}Fe_{1-x}PO_4$, we first calculate its formation energy (enthalpy), ΔH_f ($Li_{1+x}Fe_{1-x}PO_4$), which is defined as the total energy change of the following reaction,[46]

$$\Delta H_f = E_{tot}(Li_{1+x}Fe_{1-x}PO_4) - (1+x)E_{crystal}(Li) - (1-x)E_{crystal}(Fe) - E_{crystal}(P) - 2E_{gas}(O_2) \quad (1)$$

where E_{tot} ($Li_{1+x}Fe_{1-x}PO_4$) is the total energy of $Li_{1+x}Fe_{1-x}PO_4$, $E_{crystal}$ (Li), $E_{crystal}$ (Fe) and $E_{crystal}$ (P) are Li, Fe and P at their most stable phases, respectively, E_{gas} (O_2) is the energy of O_2 molecular gas. The calculated formation energies of different x values are shown in Table 1. We can see that ΔH_f ($Li_{1+x}Fe_{1-x}PO_4$) decreases with the increase of x and it is less than zero, indicating that $Li_{1+x}Fe_{1-x}PO_4$ is stable.

Phonon plays an important role in dynamic behaviors and thermal properties. Using first-principles phonon calculations,[44] the phonon band structures of $Li_{1+x}Fe_{1-x}PO_4$ are obtained. As shown in Figure 2a, there is no imaginary frequency in the phonon band structure of $LiFePO_4$, in accordance with the cognition that $LiFePO_4$ is thermodynamically stable. Imaginary frequency also doesn't appear in $Li_{1+x}Fe_{1-x}PO_4$ with x = 6.25% and 12.5% (Figure 2b and c), which further proves that $Li_{1+x}Fe_{1-x}PO_4$ (x = 6.25% and 12.5%) are thermodynamically stable. By contrast, the phonon band structure of $Li_{1+x}Fe_{1-x}PO_4$ (x = 18.75%) shows imaginary frequency (Figure 2d), which seems to contradict the result of formation energy. In fact, the formation energy is a thermal index, but the phonon band structure is a lattice dynamic index. Here, the structure conforming to the two indexes is truly thermodynamically stable. From this perspective, with the increasing content of Li-ions occupying at Fe sites, there is a limit for the x value to ensure the structural stability of $Li_{1+x}Fe_{1-x}PO_4$.

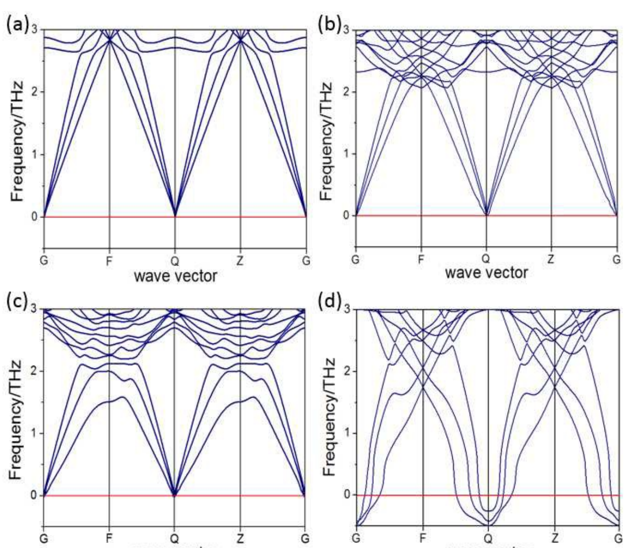

Figure 2. Phonon band structures of $Li_{1+x}Fe_{1-x}PO_4$. (a) x = 0; (b) x = 6.25%; (c) x = 12.5%; (d) x = 18.75%. Above the red line is real frequency, and below the red line is imaginary frequency.

Can the Li-rich phase introduce extra capacity?

Whether Li-rich phase $Li_{1+x}Fe_{1-x}PO_4$ is able to achieve extra capacity beyond the theoretical value of $LiFePO_4$ is an important issue we care about. The extra capacity depends on the maximum amount of Li-ions that can be extracted (also the transferable electrons). Hence, the structural stability after delithiation of $Li_{1+x}Fe_{1-x}PO_4$ is further studied. Figure 3 shows the phonon band structures of $Li_{1+x-y}Fe_{1-x}PO_4$ (x = 6.25%, y = 1-2x, 1, and 1+x). It can be seen that the structure is stable when y = 1-2x (all Fe-ions are in +3 oxidation state), but unstable when y > 1-2x.

In addition, we also performed molecular dynamics simulations to verify the instability of $Fe_{1-x}PO_4$ (x = 6.25% and 12.5%). Figure S3 provides the initial and final atomic configurations obtained at the time of 0 and 3 ps under room

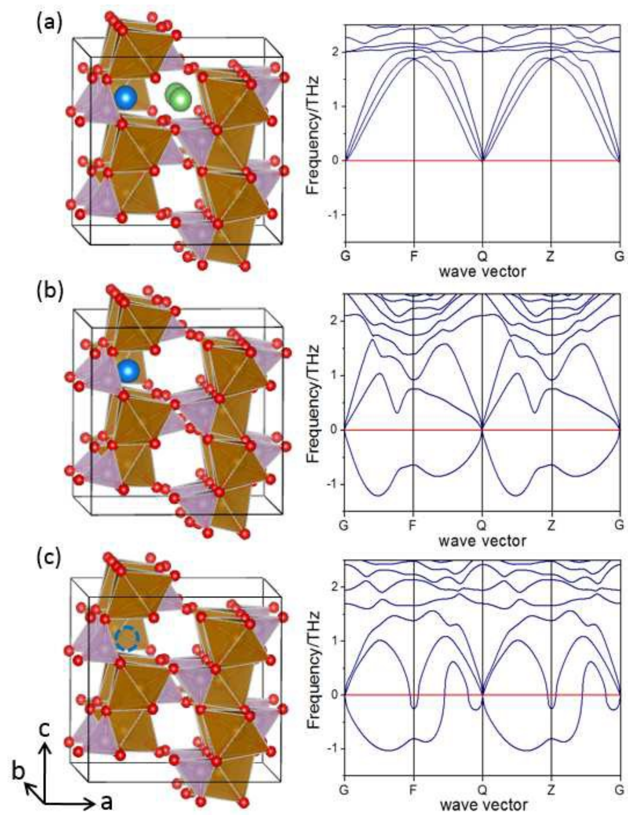

Figure 3. Schematics for structures of $Li_{1+x-y}Fe_{1-x}PO_4$ (x = 6.25%) with increasing content of delithiation and the corresponding phonon band structures. (a) y = 1-2x; (b) y = 1; (c) y = 1+x. Above the red line is real frequency, and below the red line is imaginary frequency.

View Article Online
DOI: 10.1039/C8CP01949E

temperature condition (300 K). It is obvious that some Fe-ions deviate from the original positions and the distances between the Fe-ions and their neighboring oxygen-ions become too large (3.5 Å) to form Fe-O bonds (the Fe-O bond lengths in $LiFePO_4$ don't exceed 2.3 Å). The above results suggest that $Li_{1+x}Fe_{1-x}PO_4$ (x = 6.25% and 12.5%) cannot be delithiated completely, and thus cannot enhance the specific capacity of $LiFePO_4$. This is different from our intuitive wish that the $Li_{1+x}Fe_{1-x}PO_4$ would introduce extra capacity for lithium storage, due to the good stability of the rigid polyanion framework with strong P-O covalence. We investigated the detailed reasons why Li-rich phase in $LiFePO_4$ cannot introduce extra capacity by the change of valence state of elements.

In $Li_{1+x}Fe_{1-x}PO_4$ (x = 6.25% and 12.5%), some Fe sites are occupied by Li-ions, so the valence state of Fe must change due to the charge compensation, which is confirmed by analyzing the projected electronic density of states (PDOS) of $Li_{1+x}Fe_{1-x}PO_4$. Figure 4a shows the PDOS of $LiFePO_4$. By integrating Fe 3d state (spin up and spin down) below the Fermi level, we can obtain that the magnetic moments of all

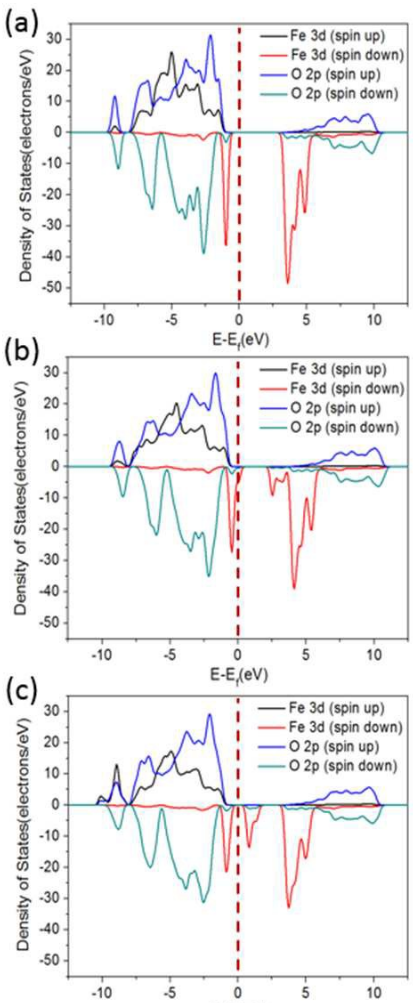

Figure 4. The PDOS of $Li_{1+x}Fe_{1-x}PO_4$. (a) x = 0; (b) x = 6.25%; (c) x = 12.5%. The Fermi level (the vertical red dashed line) is set to zero energy.

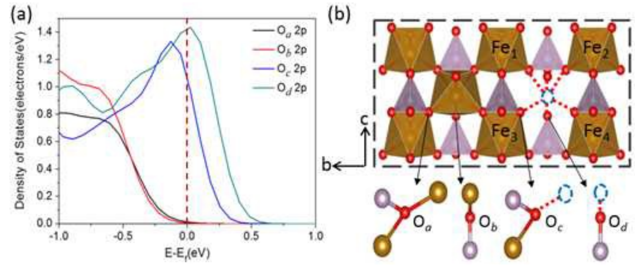

Figure 5. (a) The PDOS of O 2p orbits of four different oxygen-ion environments in $Fe_{1-x}PO_4$ (x = 6.25%). (b) The corresponding structure configurations of oxygen coordinated by Fe/P. In $FePO_4$, there are two kind of oxygen-ion environments: O_a is coordinated by 2 Fe and 1 P, O_b is coordinated by 1 Fe and 1 P. In $Fe_{1-x}PO_4$, O_a transforms into O_c, and O_b transforms into O_d around the Li-vacancy at Fe site.

Fe-ions are 3.74 μ_B, consistent with the fact that Fe-ions are in the +2 oxidation state and exhibit high spin $t_{2g}(\downarrow)t_{2g}^3(\uparrow)e_g^2(\uparrow)$ configuration in $LiFePO_4$.[47] Figure S4a shows the PDOS of $FePO_4$. The magnetic moments of all Fe-ions are 4.31 μ_B, consistent with the fact that Fe-ions are in the +3 oxidation state and exhibit high spin $t_{2g}^3(\uparrow)e_g^2(\uparrow)$ configuration in $FePO_4$. Comparing Figure 4a-c, we can see that with the increase of x, the Fe 3d state (spin down) gradually crosses the Fermi level, indicating that some Fe^{2+} ions are oxidized to Fe^{3+} state. We also calculated the magnetic moments of different Fe-ions around the excess Li-ion at Fe site for the cases of x = 6.25% and 12.5% (Figure 1c). When x is 6.25%, the magnetic moments of Fe_1, Fe_2, Fe_3 and Fe_4 are 3.74, 3.74, 4.07 and 4.07 μ_B, respectively. Interestingly, Fe_3 and Fe_4 have been oxidized but not fully to Fe^{3+}. When x is 12.5%, the magnetic moments of Fe_1, Fe_2, Fe_3 and Fe_4 are 3.74, 3.74, 4.31 and 4.31 μ_B, respectively. Obviously, Fe_3 and Fe_4 are fully oxidized to Fe^{3+}. Both at x = 6.25% and 12.5%, the oxidized Fe-ions are Fe_3 and Fe_4, not Fe_1 and Fe_2, which can also be reflected by the shorter Fe-O bond for Fe_3 and Fe_4 in Table S1.

Furthermore, we calculate the PDOS of $Li_{1+x-y}Fe_{1-x}PO_4$ (x = 6.25% and 12.5%). As shown in Figure S4, when the content of the extracted Li-ions approaches (1-2x), the Fe 3d state (spin down) fully crosses the Fermi level, meaning that all Fe^{2+} are oxidized to Fe^{3+}. When the content of the extracted Li-ions approaches (1+x), namely $Fe_{1-x}PO_4$, the O 2p state (spin up) gradually crosses the Fermi level, which means that some O-ions begin to be oxidized. Note that Figure S4 is used to illustrate how the valence state of different elements change during the delithiation of $Li_{1+x}Fe_{1-x}PO_4$, which relate to the PDOS near the Fermi level. As shown in Figure S5, during the delithiation of $Li_{1+x}Fe_{1-x}PO_4$ (x = 6.25%), the PDOS of P and Li atoms are far from the Fermi level and keep nearly unchanged. Hence, we only care about the contributions of the PDOS of Fe and O when analyzing the redox process. Figure 5 shows the PDOS of O 2p orbitals of four different oxygen-ion environments in $Fe_{1-x}PO_4$ (x = 6.25%). It can be seen clearly that O_c and O_d are oxidized, which are the O-ions bonding with the Li-ion at Fe site in $Li_{1+x}Fe_{1-x}PO_4$. So if $Li_{1+x-y}Fe_{1-x}PO_4$ (y > 1-2x) existed stably, Fe-ions would keep +3 oxidation state, and

View Article Online
DOI: 10.1039/C8CP01949E

the O-ions around the Li-vacancy at Fe site would be oxidized. The local O-ion redox would result in the fracture of the rigid framework formed by phosphate tetrahedral polyanion. This inference coincides with the above calculated phonon band structures.

In order to understand the structural instability caused by the local O-ion oxidation easily, we compared the structural distortion during delithiation. In $LiFePO_4$, FeO_6 octahedra are connected by sharing O corners to form a 2D network in *bc* plane, and the PO_4 tetrahedrons act as the joints to connect adjacent FeO_6 2D layers. The FeO_6 octahedra tend to be distorted during the cationic and anionic redox, which will also lead to the shrinkage of FeO_6 2D layers, but the PO_4 tetrahedrons between the FeO_6 2D layers would prevent this distortion and shrinkage due to the strong P-O covalence. During the process from $LiFePO_4$ to $FePO_4$ (Figure 6a), the length of Fe-O bonds shortens and lattice *a* shrinks by 4.36% (Table 2). This process is essentially a phase transition.[48] For the Li-rich phase $Li_{1+x}Fe_{1-x}PO_4$, from $Li_{1+x}Fe_{1-x}PO_4$ to $Li_{3x}Fe_{1-x}PO_4$ (x = 6.25%) with only Fe^{2+}/Fe^{3+} redox (Figure 6b), lattice *a* shrinks by 3.98% and the change of length of Fe-O bonds in the FeO_6 octahedra is similar to the phase transition from $LiFePO_4$ to $FePO_4$. However, during the oxygen-ion redox from $Li_{3x}Fe_{1-x}PO_4$ to $Fe_{1-x}PO_4$ (x = 6.25%), lattice *a* only shrinks by 0.11% and the PO_4 tetrahedrons cannot allow the shrinkage of FeO_6 2D layers any more. In addition, different from the process with only cationic redox, the length of the bond between Fe-ion and the oxidized O-ion shortens sharply during the anionic redox, indicating another kind of phase transition aggravating the structure of $Fe_{1-x}PO_4$, leading to the fracture of the pretty rigid frame structure of phosphate tetrahedral polyanion. Thus, $Li_{1+x}Fe_{1-x}PO_4$ cannot be delithiated completely, and cannot introduce extra capacity beyond the theoretical value of $LiFePO_4$.

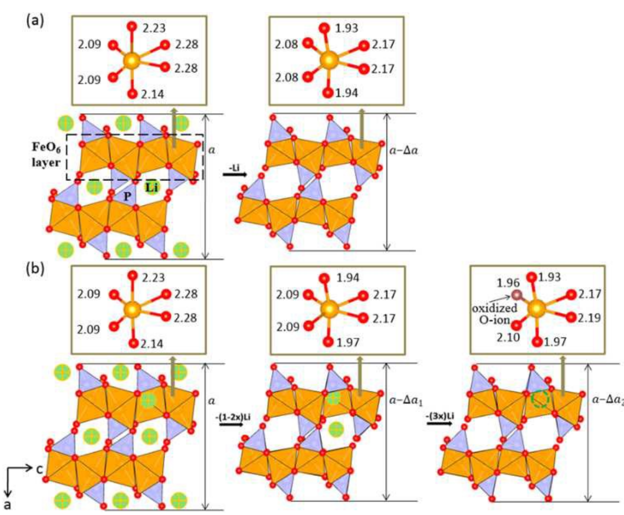

Figure 6. Full relaxed configuration for (a) $LiFePO_4$ and $FePO_4$; (b) $Li_{1+x}Fe_{1-x}PO_4$, $Li_{3x}Fe_{1-x}PO_4$ and $Fe_{1-x}PO_4$. The unit of all bond lengths is Å.

Table 2. The calculated specific change of $LiFePO_4$ and $Li_{1+x}Fe_{1-x}PO_4$ (x = 6.25%) during delithiation.

	Δ*a* [*a*]		Δ*a* [*a*]
$LiFePO_4$	0	$Li_{1+x}Fe_{1-x}PO_4$	0
$FePO_4$	4.36%	$Li_{3x}Fe_{1-x}PO_4$	3.98%
		$Fe_{1-x}PO_4$	4.09%

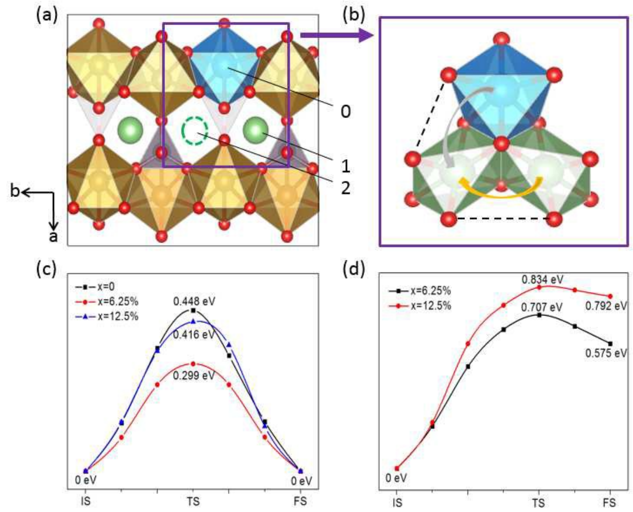

Figure 7. (a) Schematic for the structure of $Li_{1+x}Fe_{1-x}PO_4$. 1 stands for a Li-ion, and 2 stands for a Li-vacancy in the [010] channel. 0 means Li-ion at Fe site. (b) The migration pathway of Li-ion diffusion predicted by our calculations. The yellow arrow represents the path of Li-ion hoping from the 1 site to the 2 site, which is along the [010] direction through face-shared vacant tetrahedral sites. The gray arrow represents the path of Li-ion hoping from the 0 site to the 2 site, which is along the [110] direction through face-shared vacant tetrahedral sites. (c) The energy barriers for a Li-ion to hop from the 1 site to the 2 site in the bulk $Li_{1+x}Fe_{1-x}PO_4$ (x = 0, 6.25% and 12.5%). (d) The energy barriers for a Li-ion to hop from the 0 site to the 2 site in the bulk $Li_{1+x}Fe_{1-x}PO_4$ (x = 6.25% and 12.5%). IS, TS and FS represent the initial, transitional and final states, respectively.

The enhanced Li-ion diffusivity in $Li_{1+x}Fe_{1-x}PO_4$.

It is widely known that Li-ions diffuse along the [010] channel in the bulk $LiFePO_4$.[49] Li-ions hop between adjacent octahedral sites via a tetrahedron hollow formed by the edge-sharing LiO_6 octahedrons.[50] Similar migration trajectories exist in the bulk $Li_{1+x}Fe_{1-x}PO_4$ (x = 6.25% and 12.5%). As shown in Figure 7a, 1 stands for a Li-ion, and 2 stands for a Li-vacancy. The path 1-2 is the migration pathway of Li-ion diffusion along the [010] direction. In the bulk $LiFePO_4$, the barrier for a Li-ion to hop from the 1 site to the 2 site is 0.448 eV. This result is very close to 0.42 eV obtained by Christian Kuss.[51] In $Li_{1+x}Fe_{1-x}PO_4$ (x = 6.25% and 12.5%), the barriers for a Li-ion to hop from the 1 site to the 2 site are 0.299 and 0.416 eV (Figure 7c), respectively, lower than the barrier of x = 0. This indicates that the excess Li-ions at Fe sites can enhance the Li-ion diffusivity along the adjacent [010] channel, coinciding with the results obtained by Kyu-Young Park.[39] The energy barriers for Li-ion diffusion along another adjacent [010] channel are shown in Figure S6, exhibiting the same inference. The enhanced Li-ion diffusivity in $Li_{1+x}Fe_{1-x}PO_4$ along the adjacent [010] channels can be explained as following: comparing

View Article Online
DOI: 10.1039/C8CP01949E

the crystal structures of $LiFePO_4$ with $Li_{1+x}Fe_{1-x}PO_4$, the 0 site is occupied by Fe-ion in $LiFePO_4$, but is occupied by Li-ion in $Li_{1+x}Fe_{1-x}PO_4$ (x = 6.25% and 12.5%). Due to the much smaller charge of the Li-ion at Fe site, the Coulombic repulsion between the metal-ion at the 0 site and the Li-ion at the 1/2 site decreases greatly. In addition, the distance between the 1 site and the 2 site becomes shortened after Li-ions doping at Fe sites (Table S2).

Besides that, we calculated the diffusion barrier for a Li-ion hopping from the 0 site to the 2 site in the bulk $Li_{1+x}Fe_{1-x}PO_4$ (x = 6.25% and 12.5%). As shown in Figure 7d, the energy barriers are 0.707 and 0.834 eV, respectively, a little higher than the calculated result of the path 1-2, but much lower than 3.36 eV,[52] which is the energy barrier for Li-ion diffusion along the [101] direction in the bulk $LiFePO_4$. GKP Dathar pointed that when Li-Fe anti-site defects arose in $LiFePO_4$, the energy barrier for a Li-ion to hop from the Fe site to the Li site in the adjacent [010] channel varied in the range of 0.75-0.85 eV.[53] Malik *et al.* proved that Li-ion could cross over between different [010] channels and the diffusion mechanism tended to shift from 1D to 2D/3D in the presence of large concentration of anti-site defects.[54] Therefore, we can see clearly that the Li-ion at the 0 site has the ability to transfer to the 2 site, activating the shift from 1D to 2D/3D diffusion. Figure 7b summarizes the migration pathway of Li-ion diffusion predicted by our calculations. Similar to migration pathway of Li-ion diffusion along the [010] channel (yellow arrow), Li-ion at Fe site hops from the Fe site to the Li site in the adjacent [010] channel via a tetrahedron hollow formed by the edge-sharing LiO_6 octahedra (gray arrow).

Conclusions

In summary, this work presents a systematic theoretical study of Li-rich olivine phase in $LiFePO_4$. Our calculated results show that $Li_{1+x}Fe_{1-x}PO_4$ are thermodynamically stable when x does not exceed 12.5%. $Li_{1+x}Fe_{1-x}PO_4$ cannot achieve the extra capacity by anionic redox activity, because the structure becomes unstable when the content of the extracted Li-ions exceeds (1-2x). This can be attributed to that the local oxygen-ion redox will cause the fracture of the rigid frame structure formed by phosphate tetrahedral polyanion. Though the extra capacity cannot be achieved in $Li_{1+x}Fe_{1-x}PO_4$, the Li-ion diffusivity is enhanced by the excess Li-ions at Fe sites, reflected by the reduced energy barrier for the Li-ion diffusion along the adjacent [010] channel and the shift from 1D to 2D/3D diffusion. Our findings provide a fresh perspective on olivine-type $LiFePO_4$, and offer some important clues on designing Li-rich cathode materials with high energy density.

Conflicts of interest

There are no conflicts to declare.

Acknowledgements

This work was financially supported by National Materials Genome Project (2016YFB0700600), the National Natural Science Foundation of China (No. 21603007 and 51672012), and Shenzhen Science and Technology Research Grant (No. JCYJ20150729111733470 and JCYJ20151015162256516).

Notes and references

1 B. Dunn, H. Kamath, J.-M. Tarascon, *Science*, 2011, **334**, 928-935.
2 C. Masquelier, L. Croguennec, *Chem. Rev.*, 2013, **113**, 6552-6591.
3 J. Lu, Z. Chen, Z. Ma, F. Pan, L. A. Curtiss, K. Amine, *Nat. Nanotechnol.*, 2016, **11**, 1031-1038.
4 Y.-X. Yu, *J. Mater. Chem. A*, 2013, **1**, 13559-13566.
5 Y.-X. Yu, *Phys. Chem. Chem. Phys.*, 2013, **15**, 16819-16827.
6 N. Badi, *J. Mater. Sci.: Mater. Electron.*, 2016, **27**, 10342-10346.
7 J. B. Goodenough, Y. Kim, *Chem. Mater.*, 2009, **22**, 587-603.
8 Z. Lu, D. MacNeil, J. Dahn, *Electrochem. Solid-State Lett.*, 2001, **4**, A191-A194.
9 T. Ohzuku, A. Ueda, M. Nagayama, Y. Iwakoshi, H. Komori, *Electrochim. Acta*, 1993, **38**, 1159-1167.
10 H. Ren, Y. Huang, Y. Wang, Z. Li, P. Cai, Z. Peng, Y. Zhou, *Mater. Chem. Phys.*, 2009, **117**, 41-45.
11 K. Mizushima, P. Jones, P. Wiseman, J. B. Goodenough, *Mater. Res. Bull.*, 1980, **15**, 783-789.
12 D. H. Seo, J. Lee, A. Urban, R. Malik, S. Kang, G. Ceder, *Nat. Chem.*, 2016, **8**, 692-697.
13 M. Saubanère, E. McCalla, J. M. Tarascon, M. L. Doublet, *Energy Environ. Sci.*, 2016, **9**, 984-991.
14 Y. Xie, M. Saubanère, M. L. Doublet, *Energy Environ. Sci.*, 2017, **10**, 266-274.
15 H. Koga, L. Croguennec, M. Ménétrier, K. Douhil, S. Belin, L. Bourgeois, E. Suard, F. Weill, C. Delmas, *J. Electrochem. Soc.*, 2013, **160**, A786-A792.
16 M. Oishi, C. Yogi, I. Watanabe, T. Ohta, Y. Orikasa, Y. Uchimoto, Z. Ogumi, *J. Power Sources*, 2015, **276**, 89-94.
17 K. Luo, M. R. Roberts, R. Hao, N. Guerrini, D. M. Pickup, Y.-S. Liu, K. Edström, J. Guo, A. V. Chadwick, L. C. Duda, P. G. Bruce, *Nat. Chem.*, 2016, **8**, 684-691.
18 H. Chen, M. S. Islam, *Chem. Mater.*, 2016, **28**, 6656-6663.
19 R. Xiao, H. Li, L. Chen, *Chem. Mater.*, 2012, **24**, 4242-4251.
20 M. Oishi, K. Yamanaka, I. Watanabe, K. Shimoda, T. Matsunaga, H. Arai, Y. Ukyo, Y. Uchimoto, Z. Ogumi, T. Ohta, *J. Mater. Chem. A*, 2016, **4**, 9293-9302.
21 K. Luo, M. R. Roberts, N. Guerrini, N. Tapia-Ruiz, R. Hao, F. Massel, D. M. Pickup, S. Ramos, Y.-S. Liu, J. Guo, A. V. Chadwick, L. C. Duda, P. G. Bruce, *J. Am. Chem. Soc.*, 2016, **138**, 11211-11218.
22 N. Yabuuchi, M. Takeuchi, M. Nakayama, H. Shiiba, M. Ogawa, K. Nakayama, T. Ohta, D. Endo, T. Ozaki, T. Inamasu, *P. Natl. Acad. Sci. USA*, 2015, **112**, 7650-7655.
23 N. Yabuuchi, M. Nakayama, M. Takeuchi, S. Komaba, Y. Hashimoto, T. Mukai, H. Shiiba, K. Sato, Y. Kobayashi, A. Nakao, *Nat. Commun.*, 2016, **7**, 13814.
24 M. Sathiya, G. Rousse, K. Ramesha, C. Laisa, H. Vezin, M. T. Sougrati, M. Doublet, D. Foix, D. Gonbeau, W. Walker, *Nat. Mater.*, 2013, **12**, 827.
25 M. Sathiya, J.-B. Leriche, E. Salager, D. Gourier, J.-M. Tarascon, H. Vezin, *Nat. Commun.*, 2015, **6**, 6276.
26 E. McCalla, M. T. Sougrati, G. Rousse, E. J. Berg, A. Abakumov, N. Recham, K. Ramesha, M. Sathiya, R. Dominko, G. Van Tendeloo, *J. Am. Chem. Soc.*, 2015, **137**, 4804-4814.

View Article Online
DOI: 10.1039/C8CP01949E

27 S. Huang, B. E. Wilson, B. Wang, Y. Fang, K. Buffington, A. Stein, D. G. Truhlar, *J. Am. Chem. Soc.*, 2015, **137**, 10992-11003.
28 E. McCalla, A. M. Abakumov, M. Saubanère, D. Foix, E. J. Berg, G. Rousse, M.-L. Doublet, D. Gonbeau, P. Novák, G. Van Tendeloo, *Science*, 2015, **350**, 1516-1521.
29 P. E. Pearce, A. J. Perez, G. Rousse, M. Saubanère, D. Batuk, D. Foix, E. McCalla, A. M. Abakumov, G. Van Tendeloo, M.-L. Doublet, J. M. Tarascon, *Nat. Mater.*, 2017, **16**, 580-586.
30 A. J. Perez, Q. Jacquet, D. Batuk, A. Iadecola, M. Saubanère, G. Rousse, D. Larcher, H. Vezin, M.-L. Doublet, J.-M. Tarascon, *Nat. Energy*, 2017, **2**, 954.
31 J. R. Croy, M. Balasubramanian, K. G. Gallagher, A. K. Burrell, *Acc. Chem. Res.*, 2015, **48**, 2813-2821.
32 R. Benedek, H. Iddir, *J. Phys. Chem. C*, 2017, **121**, 6492-6499.
33 J. Billaud, C. Eames, N. Tapia-Ruiz, M. R. Roberts, A. J. Naylor, A. R. Armstrong, M. S. Islam, P. G. Bruce, *Adv. Energy Mater.*, 2017, **7**, 1601043.
34 T. Masese, C. Tassel, Y. Orikasa, Y. Koyama, H. Arai, N. Hayashi, J. Kim, T. Mori, K. Yamamoto, Y. Kobayashi, H. Kageyama, Z. Ogumi, Y. Uchimoto, *J. Phys. Chem. C*, 2015, **119**, 10206-10211.
35 J. B. Goodenough, K. S. Park, *J. Am. Chem. Soc.*, 2013, **135**, 1167-1176.
36 J. Zheng, Y. Hou, Y. Duan, X. Song, Y. Wei, T. Liu, J. Hu, H. Guo, Z. Zhuo, L. Liu, Z. Chang, X. Wang, D. Zherebetskyy, Y. Fang, Y. Lin, K. Xu, L. W. Wang, Y. Wu, F. Pan, *Nano Lett.*, 2015, **15**, 6102-6109.
37 L.-X. Yuan, Z.-H. Wang, W.-X. Zhang, X.-L. Hu, J.-T. Chen, Y.-H. Huang, J. B. Goodenough, *Energy Environ. Sci.*, 2011, **4**, 269-284.
38 A. Yamada, M. Hosoya, S.-C. Chung, Y. Kudo, K. Hinokuma, K.-Y. Liu, Y. Nishi, *J. Power Sources*, 2003, **119-121**, 232-238.
39 K.-Y. Park, I. Park, H. Kim, G. Yoon, H. Gwon, Y. Cho, Y. S. Yun, J.-J. Kim, S. Lee, D. Ahn, Y. Kim, H. Kim, I. Hwang, W.-S. Yoon, K. Kang, *Energy Environ. Sci.*, 2016, **9**, 2902-2915.
40 J. P. Perdew, K. Burke, M. Ernzerhof, *Phys. Rev. Lett.*, 1996, **77**, 3865-3868.
41 V. I. Anisimov, J. Zaanen, O. K. Andersen, *Phys. Rev. B*, 1991, **44**, 943-954.
42 F. Zhou, C. A. Marianetti, M. Cococcioni, D. Morgan, G. Ceder, *Phys. Rev. B*, 2004, **69**, 201101.
43 G. Henkelman, B. P. Uberuaga, H. Jonsson, *J. Chem. Phys.*, 2000, **113**, 9901-9904.
44 A. Togo, I. Tanaka, *Scr. Mater.*, 2015, **108**, 1-5.
45 G. Rousse, J. R. Carvajal, S. Patoux, C. Masquelier, *Chem. Mater.*, 2003, **15**, 4082-4090.
46 S. Chen, P. Narang, H. A. Atwater, L. W. Wang, *Adv. Mater.*, 2014, **26**, 311-315.
47 T. Maxisch, F. Zhou, G. Ceder, *Phys. Rev. B*, 2006, **73**, 104301.
48 Y. Orikasa, T. Maeda, Y. Koyama, H. Murayama, K. Fukuda, H. Tanida, H. Arai, E. Matsubara, Y. Uchimoto, Z. Ogumi, *J. Am. Chem. Soc.*, 2013, **135**, 5497-5500.
49 D. Morgan, A. Van der Ven, G. Ceder, *Electrochem. Solid-State Lett.*, 2004, **7**, A30-A32.
50 S. Nishimura, G. Kobayashi, K. Ohoyama, R. Kanno, M. Yashima, A. Yamada, *Nat. Mater.*, 2008, **7**, 707-711.
51 C. Kuss, G. Liang, S. B. Schougaard, *J. Mater. Chem.*, 2012, **22**, 24889-24893.
52 M. S. Islam, D. J. Driscoll, C. A. J. Fisher, P. R. Slater, *Chem. Mater.*, 2005, **17**, 5085-5092.
53 G. K. P. Dathar, D. Sheppard, K. J. Stevenson, G. Henkelman, *Chem. Mater.*, 2011, **23**, 4032-4037.
54 R. Malik, D. Burch, M. Bazant, G. Ceder, *Nano Lett.*, 2010, **10**, 4123-4127.